ON THE MECHANISM OF DISPERSED FLOW HEAT TRANSFER IN THE CIRCULAR BEND

F. Mayinger and M.J. Wang

Lehrstuhl A für Thermodynamik, Technische Universität München,
80290 München, FR Germany

ABSTRACT

This paper presents experimental and theoretical study of dispersed flow heat transfer in the 90-degree circular bend. Heat transfer mechanism is analyzed from measurements of phase distribution and heat transfer together with theoretical examination of single-phase flow heat transfer and droplet dynamics. It is revealed that due to the substantial change in droplet dynamics and phase distribution, dispersed flow heat transfer is remarkably improved in the bend. Two heat transfer patterns of different mechanisms are identified, namely the heat transfer under non-rewetting status and under rewetting status. The former maintains the characters of film boiling, whereas the latter is governed by partial or total liquid film evaporation.

1. INTRODUCTION

Heat transfer of dispersed flow is important in many engineering applications, e.g. in the design of once-through steam generators and in the accident analysis of nuclear reactors. Relevant mechanisms on this topic have been well studied under different boundary conditions in simple geometries (Mayinger, 1982). It is known that the wall heat transfer of fully developed dispersed flow is mainly dominated by the bulk and local vapor convection. Because of high wall superheating, dispersed droplets entrained in the vapor phase have little chance to reach the wall. Consequently, they act only as a disturbing factor to the vapor boundary layer and their contribution to the wall heat transfer is of secondary importance. For example, Lin et al. (1989) showed a less than 5% of droplet-wall heat transfer to the total heat transfer.

However, mechanism of dispersed flow heat transfer is still poorly understood in complicated flow geometries, e.g. in the circular bend – a common flow geometry in practice. Due to the occurrence of the centrifugal force and the secondary flow, dispersed flow dynamics may be subjected to changes in the bulk flow structure, droplet dynamics and phase distribution in comparison with the ones in the vertical channel. It is the aim of the present study to clarify the effects of fluid dynamic changes on the mechanism of the dispersed flow heat transfer in the circular bend.

2. METHODOLOGY

2.1. Experimental

The experiments were carried out in a refrigerant Freon-12 two-phase flow test facility illustrated in figure 1.

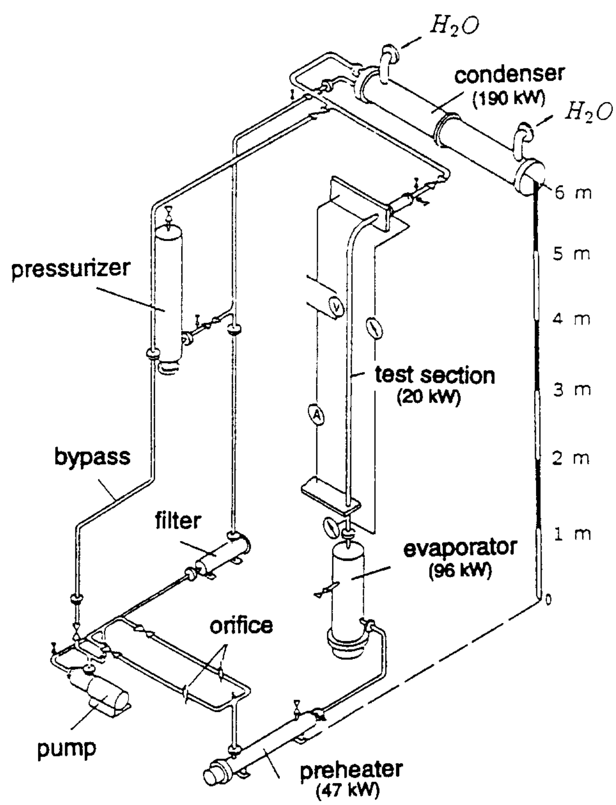

Figure 1: Sketch of refrigerant Freon-12 test loop

Dispersed flow was produced through the dryout of the annular flow in the vertical part of the Joule-heated test-section. The dryout point was regulated to occur at a position 2.5 m before the bend inlet to allow a sufficient length of dispersed flow development. The test-section shown in figure 2 consists of a vertical part and a bend. It is made of stainless steel, having an inner diameter of 28.5 mm and a wall thickness of 2.6 mm. The bend part after processing has an ellipticity smaller than 4% and a maximum deviation in wall thickness of 4.6%. Wall temperatures were measured by NiCr-Ni thermocouples of 0.5 mm diameter, spot welded on the outside surface of the tube at different axial and circumferential locations. Right after the impedance probe, two movable thermocouples were installed for assessment of fluid temperature during measurement.

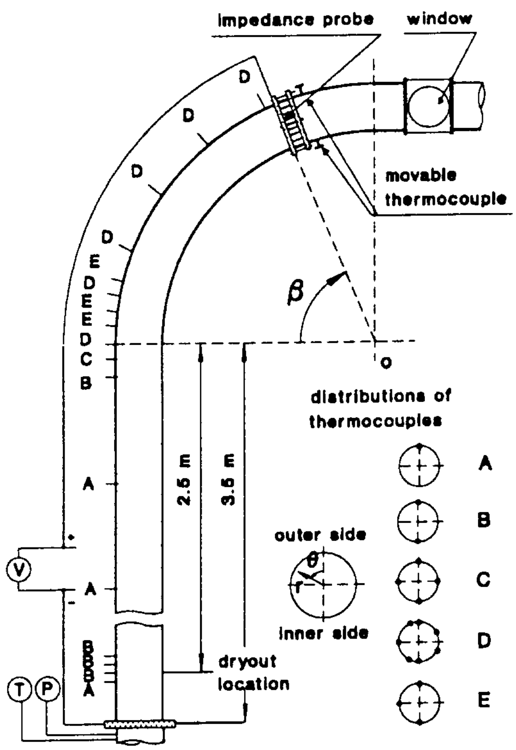

Figure 2: Layout of the test-section

An impedance probe was used to measure the local liquid fraction in five different regions of the cross-section. Figure 4 shows the structure of the probe. It is composed of four thin concentric rings divided and wired together to constitute five separate capacitors in which a nearly homogenous electric field can be established. Different capacitors were electrically isolated and supported by an epoxide frame. Supplied with 1 MHz high frequency voltage, these capacitors were measured by a high precision capacitance-meter. According to the Maxwell's theoretical analysis on dispersed droplet flow, the liquid fraction $1-\epsilon$ can be deduced from the two-phase dielectric constant e via capacitance measurement

$$1-\epsilon = \frac{e-e_g}{e+2e_g}\,\frac{e_l+2e_g}{e_l-e_g} \tag{1}$$

where e_l and e_g are the dielectric constants for pure liquid and pure gas. Wang (1993) provided an error analysis for this measuring technique. He revealed that the impedance probe gives a good indication of liquid fraction even if there is a thin liquid film forming on one of the electrodes due to the droplet impingement. For example, the relative error for liquid fraction accounts for about 9% if the liquid film occupies 10% of the total liquid.

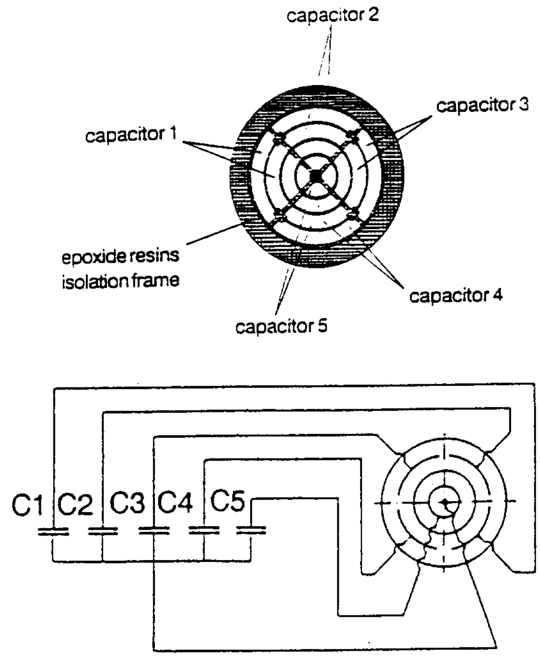

Figure 3: Structure of the impedance probe

The test conditions are summarized as follows:

mass flux G	400 - 2000 kg/m^{2}s
wall heat flux $\dot{q}_w$	20 - 60 kW/m^2
bend/tube radius ratio R_c/R	42
system pressure P	9.5 bar

2.2. Theoretical

In view of the high quality nature of dispersed flow, the heat transfer mechanism is closely connected with the behavior of the bulk vapor fields and droplet dynamics in the bend. To this end, the bulk vapor fields are numerically studied by solving the single-phase Eulerian conservation equations with appropriate boundary conditions and the standard $k-\varepsilon$ turbulence model. The computations were carried out using the finite-difference code FLOW3D (Burns &

Wilkes 1987). A modified and three-dimensional version of the Rhie & Chow algorithm was used to overcome the problem of checkerboard oscillations usually associated with the use of non-staggered grids. SIMPLEC algorithm was used for pressure-velocity decoupling, and the hybrid differencing scheme was used for the convective term. The constants used in the $k-\varepsilon$ turbulence model $C_\mu, C_1, C_2, \sigma_k, \sigma_T$ were set to be 0.09, 1.44, 1.92, 1.0 and 0.9 respectively. Standard wall functions, i.e. the log layers functions, were used near the walls. Numerical details are given in Wang (1993).

With the computed bulk vapor fields, a Lagrangian droplet trajectory model was established to study droplet dynamics in the superheated vapor stream. It is assumed that the presence of droplets does not modify the vapor fields; forces due to virtual mass, Basset history integral, pressure gradient, Saffman and Magnus lifts as well as particle interactions are negligible; and droplets remain spherical before and after impact on the wall. The path of an evaporating droplet can be thus described by the following ordinary differential energy and force balance equations:

$$h_{lg}\frac{\mathrm{d}m_d}{\mathrm{d}t} = -\dot{Q}_{gd} \tag{2}$$

$$\frac{\mathrm{d}(m_d V_{d,i} \boldsymbol{e}_i)}{\mathrm{d}t} = F_i \boldsymbol{e}_i \tag{3}$$

where m_d is the mass of the droplet and $\dot{Q}_{gd}$ is the rate of heat convection from superheated vapor to the droplet

$$\dot{Q}_{gd} = \pi d^2 \alpha_{gd}(T_g - T_s) \tag{4}$$

where d is the droplet diameter and α_{gd} is the heat transfer coefficient determined from the droplet Reynolds number Re_d, vapor film Prandtl number $Pr_{g,f}$ and the Spalding number B (Renksizbulut & Yuen, 1983)

$$\alpha_{gd} = \frac{\lambda_{g,f}}{d}(2 + 0.57 Re_d^{0.5} Pr_{g,f}^{0.33})(1+B)^{-0.7} \tag{5}$$

In equation 3, the derivative of the unit vector $\boldsymbol{e}_i$ with respect to time t is a function of the Lagrangian velocity components $V_{d,i}$ and the rest unit vectors in the toroidal coordinate system (coordinates specified in figure 2). By rearranging these derivations in the equation, the centrifugal force $\boldsymbol{F}_c$ in Lagrangian system is arrived (Wang, 1993)

$$\boldsymbol{F}_c = m_d\left(\frac{V_{d,\beta}^2 \cos\theta}{R_c + r\cos\theta}\right)e_r + m_d\left(\frac{V_{d,\beta}^2 \sin\theta}{R_c + r\cos\theta}\right)e_\theta \tag{6}$$

Other external forces are the drag force $\boldsymbol{F}_D$

$$\boldsymbol{F}_D = \frac{1}{4}\pi d^2 c_D \frac{1}{2}\varrho_g \mid \boldsymbol{V}_g - \boldsymbol{V}_d \mid (\boldsymbol{V}_g - \boldsymbol{V}_d) \tag{7}$$

where the drag coefficient c_D is calculated according to Renksizbulut & Yuen (1983)

$$c_D = \frac{24}{Re_d}(1 + 0.2 Re_d^{0.63})(1+B)^{-0.2} \tag{8}$$

the buoyancy $\boldsymbol{F}_b$

$$\boldsymbol{F}_b = \frac{1}{6}\pi d^3(\varrho_l - \varrho_g)\boldsymbol{g} \tag{9}$$

and the thermal repelling force $F_{t,r}$ due to non-uniform evaporation on the droplet surface (Ganic & Rohsenow, 1979)

$$\begin{aligned} F_{t,r} &= \iint_A V_r(\varrho_g \boldsymbol{V} d\boldsymbol{A}) \\ &= \frac{\pi d^2 {\alpha_{gd}}^2}{4 h_{fg}^2 \varrho_g}\left[(T_{g,2} - T_s)^2 - (T_{g,1} - T_s)^2\right] \end{aligned} \tag{10}$$

where V_r is the radial velocity of vapor leaving from the droplet surface, $T_{g,1}, T_{g,2}$ are the vapor temperatures at the positions corresponding to the center of the front and the rear part of the droplet in the direction to the wall.

Equations 2 and 3 for energy and force balances together with the equations for Lagrangian velocity components

$$\frac{\mathrm{d}r}{\mathrm{d}t} = V_{d,r} \tag{11}$$

$$\frac{\mathrm{d}\theta}{\mathrm{d}t} = \frac{V_{d,\theta}}{r} \tag{12}$$

$$\frac{\mathrm{d}\beta}{\mathrm{d}t} = \frac{V_{d,\beta}}{R_c + r\cos\theta} \tag{13}$$

were solved by the 4th-order Runge-Kutta algorithm.

Interactions of the droplet with the hot wall are simulated following a graphical correlation for the rebounding velocity (Bolle & Moureau, 1982). A breakup criterion based on previous experimental data is also included in the model. It is assumed that the droplet breakup number is a function of the droplet impinging Weber number, specifically, 1 for $We_i < 30$, 2 for $30 \le We_i \le 80$ and 10 for $We_i > 80$.

3. RESULTS AND DISCUSSION

3.1. Dispersed Flow Dynamics

One of the remarkable behaviors of dispersed flow dynamics in the bend is the appearance of the secondary vapor flow, illustrated by the numerical results in figure 4. It is seen that the secondary flow in a double-vortex form develops within the first 15 degrees in the bend and reaches a maximum at about 45-degree bend angle which accounts for about 9% of the mean velocity. The maximum secondary flow is limited to a narrow region close to the wall, where droplet dynamics, phase distribution and local heat transfer may be strongly influenced.

Figure 5 illustrates the thermal and fluiddynamic effects of the vapor stream on the droplet dynamics. Droplet trajectories from the Lagrangian theoretical model are presented in this figure for three droplets of different sizes. The continuous lines represent the cases with thermal effect, simulating droplet

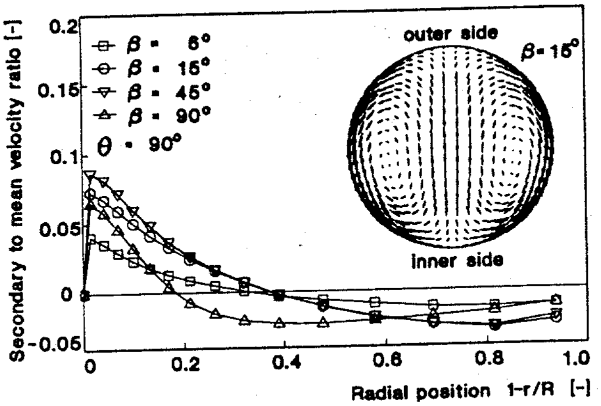

Figure 4: Secondary vapor flow in the bend at $Re = 1.07 \times 10^6$

trajectories in high-superheated flows, whereas the dotted lines represent the cases without thermal effect, corresponding to droplet trajectories in slight-superheated or equilibrium flows.

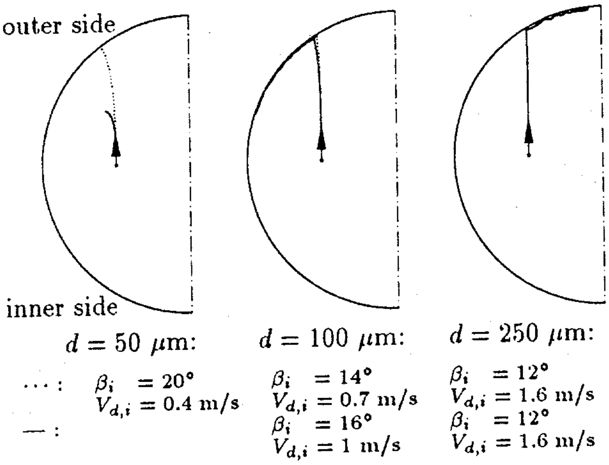

Figure 5: droplet motion in the bend: $V_g = 10$ m/s, $Re_g = 1.07 \times 10^6$, $\dot{q}_w = 60$ kW/m^2, $T_{g,0} - T_s = 80°$C

It is clearly demonstrated from the figure that except for very small droplets which soon evaporate in the superheated vapor stream, droplets usually have sufficient kinetic energy to reach the outer wall. The centrifugal forces are dominant to the droplet motion in the bulk region. The secondary reverse flow is only effective to the droplets of intermediate size (see the trajectories of $d = 100\ \mu$m). Large droplets usually break up on the outer wall, and the satellite pieces from broken bodies still tend to move towards the outer side of the symmetric plane because of the large initial momentum. As a result of droplet impact, breakup and evaporation, the degree of local thermal nonequilibrium may be greatly reduced, and consequently the local heat transfer may be enhanced.

The remarkable change of the bulk flow structure and the droplet dynamics in the bend results in the unique features of phase distribution, shown in figures 6 and 7. It is important to find from these experimental results that phase separation due to the centrifugal effect appears immediately after the bend inlet. The liquid fraction increases significantly from 0° to 15° in the outer side region whereas it decreases correspondingly in the inner side region. This process continues until 45° bend angle, where the effect of the secondary flow reversal becomes noticeable. It is seen in figure 6 that only a small amount of liquid is transported to the inner side region. In figure 7, however, a large amount of liquid appears in the inner region near the bend outlet. This fact can not be explained by the above analysis of droplet dynamics under film boiling, implying another way of liquid transportation, namely the liquid film inward reversal.

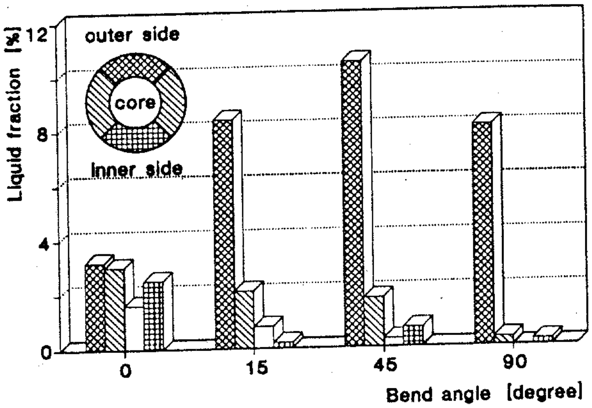

Figure 6: Phase distribution at $G = 680$ kg/m^2, $\dot{q}_w = 50$ kW/m^2

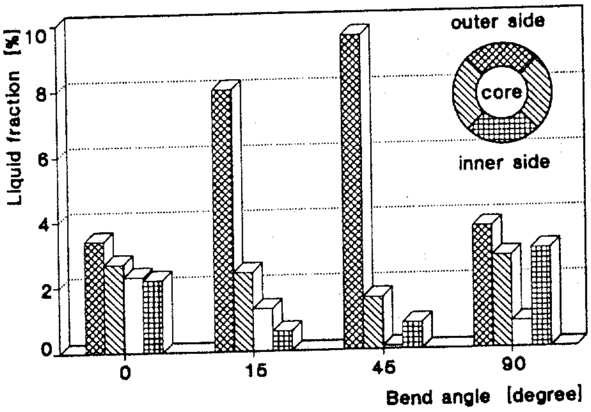

Figure 7: Phase distribution at $G = 1240$ kg/m^2, $\dot{q}_w = 30$ kW/m^2

3.2. Heat Transfer under Non-Rewetting Status

The aforementioned dynamic features of dispersed flow have a substantial impact on the heat transfer. According to whether rewetting takes place in the bend, dispersed flow heat transfer under different boundary conditions can be divided into two typical patterns. One of the patterns, namely the heat transfer under the non-rewetting status, which is usually associated with high wall heat fluxes and small mass fluxes, is analyzed here in this section.

Figure 8a shows representative measurements of wall temperature under this heat transfer pattern. Figure 8b gives an evaluation of the heat transfer coefficient from the measured values of wall temperature, mean wall heat flux and mean vapor temperature. For comparison, numerical results of single-phase flow heat transfer, together with the empirical correlation of Moshfeghian & Bell (1979) for single-phase convection are also included in figure 8b.

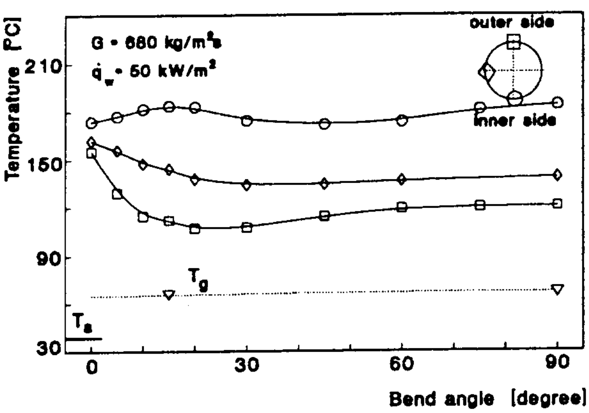

a) distribution of wall temperature

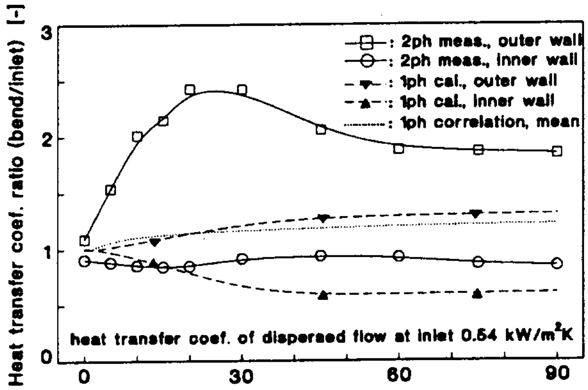

b) distribution of heat transfer coefficient

Figure 8: Heat transfer analysis under non-rewetting status

It can be seen from the figure that the bend wall is highly superheated with the temperature beyond the Leidenfrost point. No liquid droplets in this case can keep a stable contact with the wall, similar to the case in vertical film boiling. However, shortly after the bend inlet, heat transfer is remarkably improved on the outer wall and is deteriorated slightly on the inner wall. The former can be about 2 to 3 times larger than that at the bend inlet, revealing the dominant effect of droplet-wall interactions over the weak effect of vapor acceleration. The latter is due to the vapor deceleration and the phase separation induced liquid deficiency. While the secondary flow effect to the inner wall cooling is not significant for singe-phase flow, such effect is noticeable for dispersed flow heat transfer in the middle stage of the bend. As seen, the inner wall temperature decreases and the local heat transfer coefficient increases, due to the fact that the secondary flow brings not only the vapor coolant to the inner region, but also a small amount of liquid droplets that act as local heat sinks. In the later stage of the bend, droplets lose considerable momentum, and droplet-wall interactions are less effective to the wall heat transfer. The contribution of vapor convection to the wall heat transfer then becomes important. Heat transfer coefficient on either the outer or inner wall is reduced correspondingly.

3.3. Heat Transfer under Rewetting Status

Under intermediate to large mass fluxes and low heat fluxes, a stable wall temperature near the saturation line appears on the bend wall, forming another typical pattern of heat transfer, namely the heat transfer under rewetting status. Similar to the previous picture, figure 9 shows representative measurements of wall temperature and the heat transfer coefficient. Because of the weak thermal nonequilibrium of the flows under these conditions (Wang, 1993), saturation temperature is used in the evaluation of heat transfer coefficient.

As seen from the figure, due to the massive droplet impingement, the outer wall is quickly quenched to a value near the saturation temperature resulting in an order-of-magnitude increase of heat transfer coefficient. Such a dramatic increase of heat transfer indicates a departure of the heat transfer mechanism from film boiling. Under low wall superheat, droplets maintain stable contact on the outer wall where they can easily link together to form a continuous liquid film. This has been confirmed from liquid fraction measurement in figure 7. Therefore liquid film evaporation is responsible for the heat transfer augmentation. Further downstream, because of the action of the secondary flow and the gravity, rewetting is propagated from the outer side to the inner side where small wall-superheat and high liquid fraction are observed. Local heat transfer is consequently greatly enhanced.

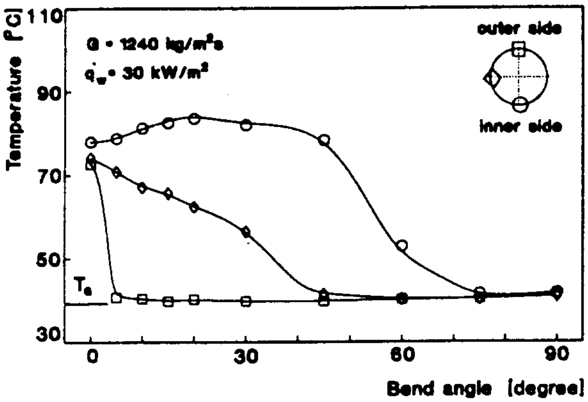

a) distribution of wall temperature

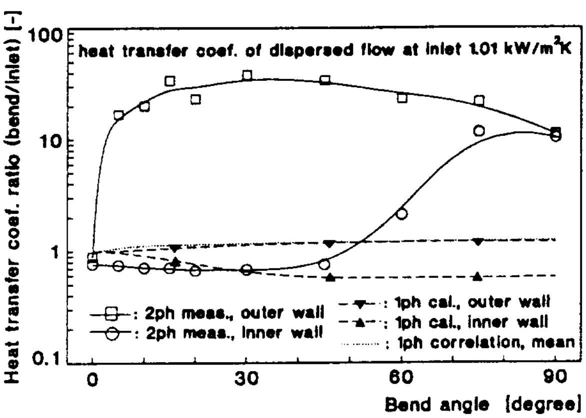

b) distribution of heat transfer coefficient

Figure 9: Heat transfer analysis under rewetting status

3.4. Transition of Heat Transfer Pattern

Transition of dispersed flow heat transfer from one pattern to another depends mainly on two factors.

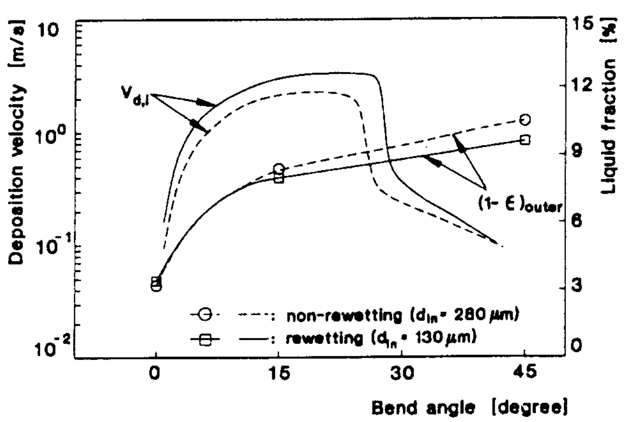

Figure 10: Analysis of droplet deposition flux

One is the temperature gradient in the boundary layer, which is coupled with wall heat flux. Another is the liquid deposition flux, which is critically influenced by the mass flux. Figure 10 shows the evaluation of droplet deposition flux on the outer wall under the same conditions as in figures 7 and 8. Although the liquid fractions in these two cases are nearly the same in the outer region, the deposition velocity of the larger mass flux is remarkably larger than that of the smaller mass flux. Therefore transition to the wetting status occurs due to the higher deposition flux of droplets under the larger mass flux.

4. CONCLUSIONS

Two different heat transfer patterns of dispersed flow are revealed and discussed from the theoretical analysis and measurements. Under the non-rewetting status, heat transfer maintains the features of film boiling. Heat transfer improvement is due to droplet impaction and vapor convection, with a more dependent upon the former. Under rewetting status, heat transfer is dramatically improved due to partial or total liquid film evaporation. The transition of the heat transfer pattern depends on the temperature gradient in boundary layer and the droplet deposition flux.

REFERENCES

Bolle, L. & Moureau, J.C. 1982, Spray Cooling of Hot Surface, in Multiphase Science and Technology, edts G.F. Hewitt, et al., vol. 1, pp. 1-98, Hemisphere, Washington.

Burns, A.D. & Wilkes, N.S. 1987, A Finite Difference Method for the Computation of Flows in Complex Three-Dimensional Geometries, UKAEA Report No. AERE-R12342.

Ganic, E.N. & Rohsenow, W.M. 1979, On the Mechanism of Liquid Drop Deposition in Two-Phase Dispersed Flow, J. of Heat Transfer, vol. 101, pp. 288-294.

Lin, T.F., Jou, J.F. & Hwang, C.H. 1989, Turbulent Forced Convection Heat Transfer in Two-Phase Evaporating Droplet Flow Through a Vertical Pipe, Int. J. Multiphase Flow, vol. 15, pp. 997-1009.

Mayinger, F. 1982, Strömung und Wärmeübertragung in Gas-Flüssigkeits-Gemischen, Springer Verlag, Wien.

Moshfeghian, M & Bell, K.J. 1979, Local Heat Transfer Measurements in and downstream from a U-Bend, ASME Paper No. 79-HT-82.

Renksizbulut, M. & Yuen, M.C. 1983, Experimental Study of Droplet Evaporation in a High-Temperature Air Stream, J. Heat Transfer, vol. 105, pp. 384-388.

Wang, M.J. 1993, Phasenverteilung, Sekundärströmung und Wärmeübergang bei Sprühkühlung in Krümmern, Dissertation, TU München.